**Youyuan Wang [1], Dawei Zhang [1] ,Guojun Lu [2], Yanguang Huang [2]**

State Key Laboratory of Power Transmission Equipment & System Security and New Technology (Chongqing University) (1)
Testing and Research Institute, Guangzhou Power Supply Bureau (2)

# Suppression method of partial-discharge interference signal based on the combination of morphological filters and complex wavelet transform

***Abstract:*** *Solving the periodic narrowband interference and suppression of white noise during the actual detection of partial discharge (PD) are difficult. In this paper, a method of suppressing the interference signal method based on the combination of morphological filters and complex wavelet transform is proposed. Generalized morphological filters based on the principle of mathematical morphology were structured and set as a pre-filter unit to realize pre-treatment of the original PD signals, and complex wavelet transform was then employed to process the PD signals. Finally, denoised PD signals were obtained. Applying this method to deal with the noise in the simulation and acquisition of PD signals, the results showed that the method can restrain effectively the PD periodic narrowband interference and white noise. Compared with the same wavelet base of the wavelet and the complex wavelet denoising methods, this method reduces energy loss and retains well the PD signals characteristics.*

***Streszczenie:*** *W artykule opisano metodę tłumienia zakłóceń (zakłócenia wąskopasmowe, biały szum) w sygnałach, w przypadku wykrycia wyładowań niezupełnych. W rozwiązaniu wykorzystano kombinację filtrów morfologicznych, działających jako pre-filtr i złożoną transformatę falkową do dalszej obróbki sygnałów. Wykonano badania symulacyjne, potwierdzające skuteczność filtracji. (**Tłumienie zakłóceń od pochodzących od wyładowań niezupełnych – filtry morfologiczne i złożona transformata falkowa**).*

**Keywords**: narrowband interference, white noise, mathematical morphology, complex wavelet transform, suppression method.
**Słowa kluczowe**: zakłócenia wąskopasmowe, biały szum, morfologia matematyczna, złożona transformata falkowa, metoda tłumienia.

## Introduction

High-voltage electrical equipment partial-discharge (PD) detection is the key in obtaining real and effective PD signals [1]. Field detection of PD signals is very weak and is often overwhelmed by surrounding interference signal, leading to serious distortion in the PD signal-detected waveform and presenting great difficulties in PD detection. Therefore, effective suppression of interference signals is vital.

The frequency characteristics of interference signals can be divided into periodic narrowband interference, random-pulse interference, and white noise. The periodic narrowband interference mainly includes power system, carrier communication, and high-frequency protection signal interferences caused by radio interference. Such interference waveform is usually a sine wave with a fixed resonant frequency and bandwidth [2]. The random-pulse interference waveform is very similar to a PD waveform [3], which includes corona discharge at the high-voltage side of electrical equipment, pulse interference caused by grid switching, and closing or disconnecting silicon controlled rectifier device [4]. White noise is primarily caused by the thermal noise of the device [5].

Currently, interference signal suppression methods include the following: digital filter based on Fourier transform method [6], threshold filtering method based on wavelet transform [7], a combination algorithm based on morphological filter and Fourier transform [8], a combination algorithm based on morphological filter and wavelet transform [9], and so on. The digital filter method based on the Fourier transform results in higher energy loss to the original signal, and when new narrowband interference appears or the interfering signal center frequency changes, the parameters of the filter becomes invalid. The threshold filtering method based on wavelet transform can effectively suppress narrowband cycle interference and white noise, but some defects are still present, such as band aliasing, leakage effects, serious loss of the original signal energy, and difficulties in the integrity of parameters. For the combination algorithm based on morphological filter and Fourier transform and the combination algorithm based on morphological filter and wavelet transform, the denoising effect is better than that of a single-filter algorithm. However, the former has a large energy loss and less effective noise suppression, whereas in the latter, signal distortion is more serious, and the stability is not satisfactory.

This paper presents a combination of the morphological filter and complex wavelet transform as interference signal-suppression method. The method uses non-linear mathematical morphological filters as PD narrowband periodic interference pre-filter unit. It inhibits periodic narrowband interference and white noise using complex compactly supported biorthogonal wavelets. The results of denoising of the PD signals from simulation and the field indicated that this method can effectively suppress periodic narrowband interference and white noise.

## Morphological Filters Based on Mathematical Morphology

### *(A). Basic Principle of Mathematical Morphology*

Mathematical morphology [10] is a digital image processing method, whose basic idea is the search for information using a probe, called structural element. When the probe moves, the mutual relationship among various parts can be examined. These probes can directly gather knowledge to detect the structural characteristics. Grayscale images are generally used to define a real-valued function on a continuous or digital space. For the PD signals, the sampling signal is simply a real-value of a corresponding function; thus, it can be a gray morphological transform that analyzes and process the signal.

Mathematical morphology contains four basic operations, namely, expansion, corrosion, morphological opening, and morphological closing. f (n) is defined in {0, 1, 2,..... , N-1} of the original signal in one dimension, g (N) is defined in {0, 1, 2,..... , M-1} structural elements, and their origin is defined as zero. The f (n) of the inflation and corrosion operations on g (n) is expressed in Eqs. (1) and (2).

$$(f \oplus g)(n) = \max_{\substack{m=0,1,\ldots,M-1 \\ n=0,1,\ldots,N+M-2}} \{f(n-m)+g(m)\} \quad (1)$$

(2) $$(f\Theta g)(n)=\min_{\substack{m=0,1,\ldots,M-1\\ n=0,1,\ldots,N-M}}\{f(n+m)-g(m)\}.$$

By combining dilation and erosion, f (n) of the morphological opening and closing operations on g (n) can be obtained, as expressed by Eqs. (3) and (4), respectively.

(3) $$(f\circ g)(n)=((f\Theta g)\oplus g)(n)$$

(4) $$(f\bullet g)(n)=((f\oplus g)\Theta g)(n).$$

The fundamental role of the opening and closing operations is image smoothing. The opening operation eliminates the peak noise, removes the signal edge of the isolated spots and glitches, and inhibits positive pulse signal. The closing operation suppresses and eliminates the trough noise, fills crack and loophole signals, and inhibits negative pulse signals. Therefore, PD signals in narrowband interference can be removed effectively by selecting the most appropriately constructed structural element morphological filter. In particular, when the interference frequency band is wider and overlaps with the fundamental frequency, better filter characteristics can be obtained.

*(B). Structure of the Morphological Filters*

Morphological filters are based on the morphological opening and closing operations, which can be used to construct open–close filters, close–open filters, hybrid filters, and alternating hybrid filters, such as those shown by Eqs. (5)–(8).

(5) $$[(f)oc(g)](n)=(f\circ g\bullet g)(n)$$

(6) $$[(f)co(g)](n)=(f\bullet g\circ g)(n)$$

(7) $$[(f)hf(g)](n)=\frac{(f\circ g+f\bullet g)(n)}{2}$$

(8) $$[(f)ah(g)](n)=\frac{[(f)oc(g)+(f)co(g)](n)}{2}.$$

Here, oc and co are close–open and open–close alternating filter operations, hf stands for hybrid filter operation, and ah represents alternating hybrid filter operation.

Shrinkage in the opening operation in the open–close filter causes a decrease in its output, whereas expansion in the closing operation in the close–open filter leads to increase in its output amplitude, resulting in migration phenomenon of positive and negative pulse statistics in the two filters and suppression of the noise effect. Therefore, open–close and close–open filters consisting of alternating hybrid filter can be used to filter white noise and pulse noise, as defined in Eq. (9).

(9) $$F(n)=\frac{\{[(f)oc(g)](n)+[(f)co(g)](n)\}}{2}$$

*(C). Selection of Structural Elements*

Morphological filtering depends not only on the morphological transformation of the form but also on the size and shape of the structural elements. Only the size and shape of the structural elements that match the signal can be maintained.

The geometrical shapes of the structural elements are generally very simple, such as flat (straight line) and convex (circle or triangle) structural elements. The dilation and erosion operations of the flat structural elements [11] assume the local maximum and minimum values and very effectively suppress the narrowband periodic interference and white noise in the PD signals. Therefore, the constructed flat structural element morphological filter is selected.

For the morphological filter, the longer the structural element is and the more complex the shape is, the larger is the amount of computation. Usually, the length of the structural elements is less than the minimum cycle of the useful signal waveform but greater than the length of the noise. By analyzing the length of the PD signal and the noise, the ultimate length of the structural elements is 5.

**Integration of Morphological Filter and Complex Wavelet Transform Denoising Methods**

*(A). Structure of Complex Compactly Supported Biorthogonal Wavelets*

Wavelet filter h(n), g(n) is related to the amplitude–frequency characteristics only and is independent of the phase–frequency characteristics. When filter h (n), g (n) satisfies the complex biorthogonal wavelet conditions, the filter is a complex wavelet filter [12, 13]. Therefore, by maintaining the amplitude–frequency characteristics of a real wavelet filter, a change in its phase–frequency characteristics can be obtained having the same characteristics as that of the complex wavelet (biorthogonal, compactly supported, vanishing moments, regular, and so on). Usually, filter h (n) can be expressed by Z transformation, as shown in Eq. (10). Its complex roots change the wavelet phase–frequency characteristics, and its real roots only change the symmetry of the wavelet filter coefficients.

(10) $$\hat{h}(z)=h_0\left(\frac{1+z}{2}\right)^p\prod_{i=1}^{L}(z-\lambda_i)\prod_{i=1}^{M}(z-z_i)(z-z_i^*)$$

where h0 is a real number, p = 0, 1, 2, ..., $\lambda_i$ is a real number not equal to $\pm1$, $z_i$ and $z_i^*$ are complex conjugates, and h is the number of items for P + L +2M +1.

Thus, the available $z_i^*z-1$ instead of $z-z_i$ or the available $z_iz-1$ instead of $z-z_i^*$ realizes the structure of a complex wavelet. According to Ref. [13], using the db series in the wavelet processing of PD signals is better, and the processing capacity of the db series of the db4 wavelet is the best.

*(B). Selection Threshold*

According to Ref. [14], using soft or hard thresholding method in complex wavelet transform can remove most of the noise, but when the energy distribution characteristics of signal itself is considered, each sub-band denoising becomes imbalance, which is not conducive to signal reconstruction. Therefore, this paper adopts the hierarchical role of the threshold to avoid this problem.

*(C). Denoising Steps*

Setting signal f (n) as s (n) after noise pollution, s (n) = f (n) + q (n) + δ (n), where q (n) is the periodic narrowband interference signals and δ(n) is the Gaussian white noise. The signal after denoising is $f'$. Figure 1 shows the integrated morphological filters and the complex wavelet transform denoising algorithm flowchart. The specific denoising process is as follows:

(1) A set of strobe signals is obtained by morphological filtering of the noisy time-domain signal s (n).

(2) By performing complex wavelet transform of the filtered signal from Step (1), a set of complex wavelet coefficients is obtained.

(3) Based on the features of each complex wavelet coefficient layer, the threshold is considered as the real and imaginary parts of the each layer of the complex wavelet coefficients (layered after threshold).

(4) The complex wavelet coefficients, whose layered complex threshold approach have been performed, are inversely transformed; thus, complex signal WTR + iWTI is obtained.

5) By processing the composite information of WTR and WTI, denoising result $f'$ is finally obtained.

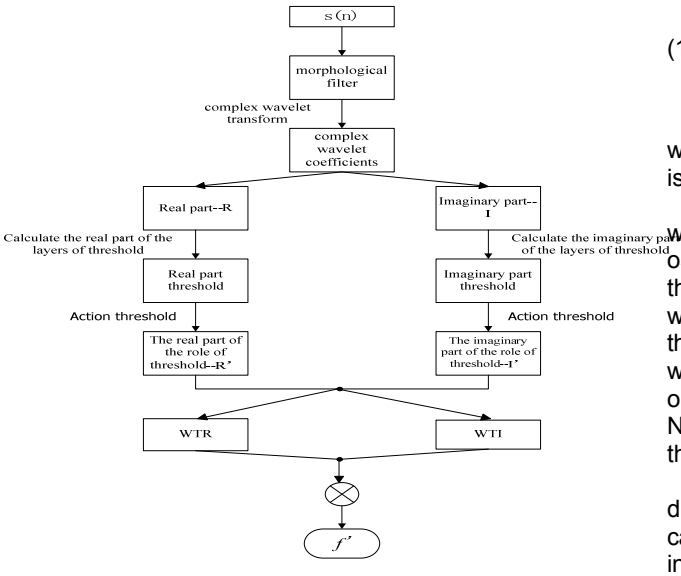


Fig. 1 Denoising algorithm flowchart

*(D). Denoising Effect Parameter Evaluation*

To evaluate the effect of the combined morphological filter and complex wavelet transform denoising method, three evaluation parameters are introduced: signal-to-noise ratio (SNR) [15], normalized correlation coefficient (NCC ) [16], and variation trend parameter (VTP) [17], defined by Eqs. (11)–(13), respectively.

$$SNR(dB) = 20 \times \lg \frac{\max\limits_{i=1,2,..,\ N} s(i)}{\max\limits_{i=1,2,..,\ N} n(i)} \tag{11}$$

where s (i) is the PD signal and n (i) is the noise signal. When SNR is positive, the signal is stronger than the noise; otherwise, the signal is weaker than the noise. Higher SNR indicates that the denoising algorithm has stronger ability to extract the signals effectively.

$$NCC = \frac{\sum_{n=1}^{N} s(n) \cdot f(n)}{\sqrt{\left(\sum_{n=1}^{N} s^2(n)\right) \cdot \left(\sum_{n=0}^{N-1} f^2(n)\right)}} \tag{12}$$

where s is the original signal and f is the denoised signal. The value of NCC is between -1 and 1, where -1 represents before and after the transformed waveform reversal, 0 represents two biorthogonal waveform, and 1 indicates exactly the same waveform. A waveform with a large NCC does not always have a high amplitude because NCC only describes the degree of similarity between two waveforms, irrespective of the waveform amplitude and energy attenuation.

VTP consists of rise VTP (RVTP) and fall VTP (FVTP), equal to the mean of the rising and falling parameter trends.

$$\mathrm{VTP} = \frac{\mathrm{RVTP} + \mathrm{FVTP}}{2} \tag{13}$$

$$RVTP = \frac{\sum_{i=2}^{N} [f(i) - f(i-1)]}{\sum_{i=2}^{N} [s(i) - s(i-1)]} \tag{14}$$

where s (i) is a waveform and f (i) is another waveform. s (i) is greater than s (i-1), and f (i) is greater than f (i-1).

$$FVTP = \frac{\sum_{i=2}^{N} [f(i-1) - f(i)]}{\sum_{i=2}^{N} [s(i-1) - s(i)]} \tag{15}$$

where s (i) is a waveform and f (i) is another waveform. s (i) is less than s (i-1), and f (i) is less than f (i-1).

VTP represents the degree of similarity trend of the two waveforms and, to some extent, measures the waveform oscillations. The closer VTP is to one, the more similar is the oscillation of the two waveforms. If the original waveform oscillates and the denoised waveform does not, then the denoising trend before and after the two waveforms is different, i.e., the VTP value is not close to one. To make up for the shortcoming of NCC, both VTP and NCC can be used to evaluate better the similarity degree of the waveforms before and after denoising.

Obtaining PD signal from the original waveform is difficult; thus, the SNR, NCC, and VTP of denoised signal cannot also be obtained. Therefore, noise suppression is introduced to evaluate the advantage and disadvantage of the denoising effect using $\sigma_1^2 = P_{u1}$ and $\sigma_2^2 = P_{u2}$, as defined in Eq. (16) [5].

$$\rho_{NRR} = 10(\lg \sigma_1^2 - \lg \sigma_2^2) = 10(\lg P_{u1} - \lg P_{u2}) \tag{16}$$

where Pu1 and Pu2 are the noise power before and after the treatment, respectively, and $\sigma_1$ and $\sigma_2$ are the deviation of the interference noise before and after noise removal, respectively. $\rho_{NRR}$ shows the highlight level of the signal after suppression of the interference. Larger $\rho_{NRR}$ indicates stronger ability to remove the PD noise.

**Analysis of the Analog Signal Denoisng of PD**

*(A). Source Simulation of the PD Signal*

Most of the detected PD signals in engineering practice are decaying oscillation signals. Equations (17)–(20), namely, single-exponential decay pulse, double-exponential decay pulse, single-exponential decay of the oscillation pulse, and double-exponential decay of the oscillation pulse, are usually used for the theoretical study of PD signals.

Model 1: Single-exponential decay pulse

$$s_1 = Ae^{-t/\tau} \tag{17}$$

Model 2: Double-exponential decay pulse

$$s_2 = A(e^{-t/\tau_1} - e^{-t/\tau_2}) \tag{18}$$

Model 3: Single-exponential decay of the oscillation pulse

$$s_3 = Ae^{-t/\tau} \sin(2\pi f_c t) \tag{19}$$

Model 4: Double-exponential decay of the oscillation pulse

$$s_4 = A(e^{-t/\tau_1} - e^{-t/\tau_2}) \sin(2\pi f_c t) \tag{20}$$

where A is the amplitude of the pulse signal, $\tau$ is the decay constant, and $f_c$ is the oscillation frequency.

These four function models can be used to simulate the PD source, as shown in Fig. 2. White noise is described using mean value u=0 and the variance ( $\sigma^2 = \zeta$ ) of a wide stationary Gaussian random process n(k). The periodic narrowband interference waveform is a sine wave, simulated by superimposing multiple sine waves. We assume that the narrowband interference signal is

superimposed by equal-amplitude sine waves of 80 kHz, 120 kHz, 265 kHz, 327 kHz, 450 kHz, 560 kHz, 620 kHz, 750 kHz, 1 MHz, and 2 MHz. The number of sampling points is 10,000, the sampling interval is 0.05 μs, and the equivalent sampling frequency is 20 MHz. Figure 2(b)–(e) shows the stained noise signal superimposed above the white noise and periodic narrowband interference. Figure 2(b) and (c) shows that the amplitude of the noise signal is larger than that of the PD signal. Figure 2(d) and (e) shows that the amplitude of the noise signal is smaller than that of the PD signal. The SNRs are 0 and -6.02 dB, respectively.

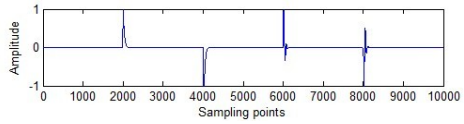


(a) Original waveform

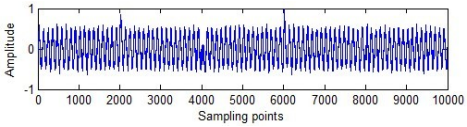


(b) Dying noise waveform (SNR=0 dB)

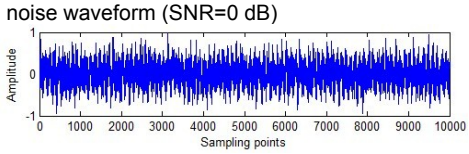


(c) Dying noise waveform (SNR=-6.02 dB)

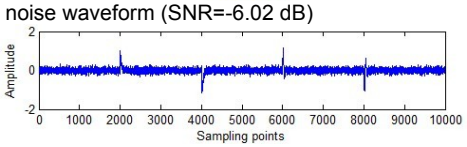


(d) Dying noise waveform (SNR=0 dB)

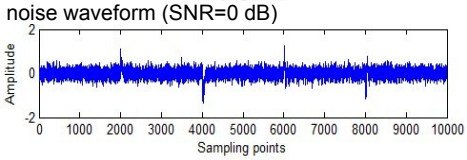


(e) Dying noise waveform (SNR=-6.02 dB)
Fig. 2 PD signal simulation

*(B). Analysis of Denoising Effect*

The wavelet transform of the wavelet, complex wavelet transform, and morphological filters were applied to the complex wavelet transform to analyze the denoising effect, as shown in Fig. 2(b) and (c). The denoising results are shown in Figs. 3 and 4. Figures 3–6 respectively show the denoising results from Fig. 2(b)–(d). Figures 3(a) and 6(a) respectively show the morphological–complex wavelet denoising results. Figures 3(b) and 6(b) respectively shows the complex wavelet denoising results, whereas Figs. 3(c) and 6(c) show the wavelet denoising results. Figures 3–6 show that, regardless whether the amplitude of the noise is larger or smaller than that of the PD signal, the denoising results of the morphological–complex wavelet are better than the other two denoising methods, indicating that this method has a strong denoising ability. It can retain much of the original signal energy while experiencing lesser distortion. The complex wavelet using the same wavelet basis can be very effective in removing noise, but the energy loss and distortion cannot be ignored. The energy distortion in the wavelet denoising is relatively small, but when the amplitude of the noise is large, distinguishing the PD signal from the denoising results becomes difficult.

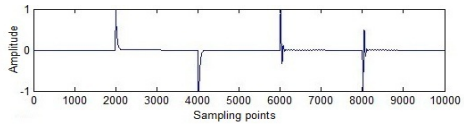


(a) Results of morphological–complex wavelet denoising

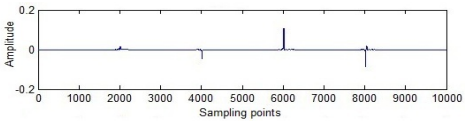


(b) Results of the complex wavelet denoising

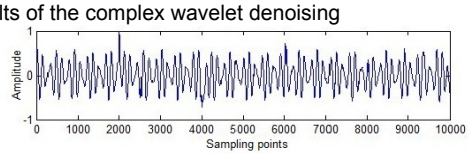


(c) Results of wavelet denoising
Fig. 3 PD signal (δ=0 dB) denoising results

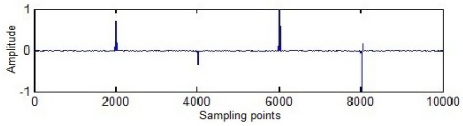


(a) Results of morphological–complex wavelet denoising

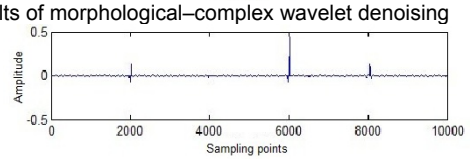


(b) Results of complex wavelet denoising

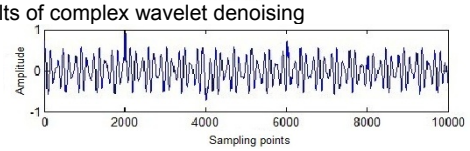


(c) Results of wavelet denoising
Fig. 4 PD signal (δ=-6.02 dB) denoising results

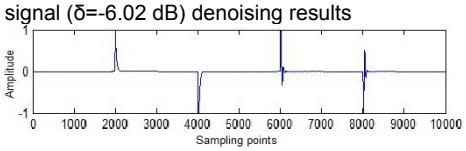


(a) Results of morphological–complex wavelet denoising

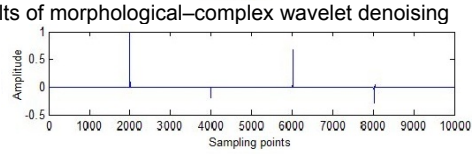


(b) Results of complex wavelet denoising

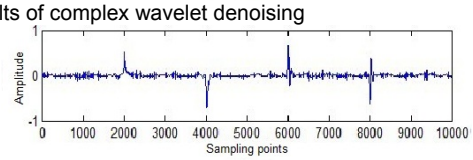


(c) Results of wavelet denoising
Fig. 5 PD signal (δ=0 dB) denoising results

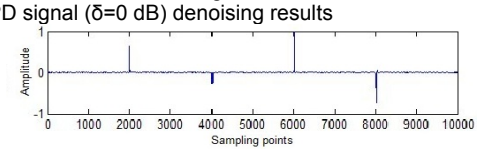


(a) Results of morphological–complex wavelet denoising

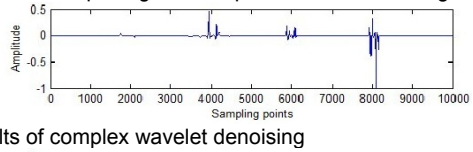


(b) Results of complex wavelet denoising

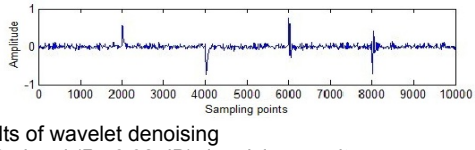


(c) Results of wavelet denoising
Fig. 6 PD signal (δ=-6.02 dB) denoising results

The evaluation results are shown in Table 1, where the amplitude of the noise is larger than that of the PD signal. Table 2 shows the evaluation results, where the amplitude of the noise is smaller than that of the PD signal. Tables 1 and 2 show that the SNR from the integration of

morphological filter and complex wavelet denoising results is the highest among the denoising methods, and its NCC is also higher than the other two methods. Therefore, compared with the complex wavelet and wavelet denoising, the morphological filter–complex wavelet denoising has better ability to extract PD signals, and the similarity of the waveforms is higher. Table 1 shows that the VTPs of the wavelet and complex wavelet denoising results are similar, but the VTP of the morphological filter–complex wavelet denoising results is larger than those obtained by the other two methods. In Table 2, the VTP of the morphological filter–complex wavelet and the wavelet denoising results shows little difference, whereas both VTPs of the morphological filter–complex wavelet and wavelet are larger than the complex wavelet. This result shows that, based on the degree of similarity in wave oscillations, the denoising results of the morphological filter–complex wavelet are better than the other two methods.

Table 1 Evaluation parameters of the denoising results

| Signal intensity | Denoising method | SNR | NCC | VTP |
|---|---|---|---|---|
| 0 dB | a | 37.3462 | 0.9102 | 0.8519 |
| | b | 30.4357 | 0.7536 | 0.8217 |
| | c | 15.4735 | 0.8437 | 0.8013 |
| -6.02 dB | a | 29.5410 | 0.8932 | 0.8435 |
| | b | 20.3487 | 0.7436 | 0.8124 |
| | c | 6.3424 | 0.7864 | 0.8156 |

Table 2 Evaluation parameters of the denoising results

| Signal intensity | Denoising method | SNR | NCC | VTP |
|---|---|---|---|---|
| 0 dB | a | 62.0317 | 0.9435 | 0.8714 |
| | b | 53.2365 | 0.8926 | 0.8462 |
| | c | 41.5834 | 0.9135 | 0.8251 |
| -6.02 dB | a | 51.7326 | 0.9203 | 0.8512 |
| | b | 32.4973 | 0.8261 | 0.8219 |
| | c | 35.6285 | 0.9072 | 0.8308 |

Therefore, applying morphological filter–complex wavelet to remove the noise in PD signals is feasible and effective. Regardless whether the amplitude of the noise signal is greater than (or less than) the amplitude of the PD signal, the denoising results of the morphological filters–complex wavelet are better than the other two methods.

**Analysis of the Denoising Results of Measured PD Signal**

*(A). Denoising Results of the Measured Signal in Laboratory*

We use only the internal (air gap) discharge model for PD signal noise analysis in the laboratory. The stained noise signal, which is not mixed with any noise during the experiment, is shown in Fig. 7. PD signal waveforms can be seen from the collected signal. Figure 9 shows the collected signal when it is mixed with 98 MHz FM and 425 MHz walkie-talkie interference signals. Obviously, the PD signal is disturbed by the noise signal. The denoised PD signal waveforms are shown in Figs. 8 and 10.

Figures 8 and 10 show that the distortion of the morphological filters–complex wavelet is relatively small; thus, the original signal is well protected. The denoising results of the complex wavelet have relatively larger distortions. For the wavelet denoising, when the amplitude of the PD signal is higher than the amplitude of the noise, this method can be used to extract PD signals. However, when the amplitude of the PD signal becomes lower than the noise, distinguishing the useful signal from the stained noise is significantly difficult. Therefore, using the morphological filters–complex wavelet is effective in removing noise.

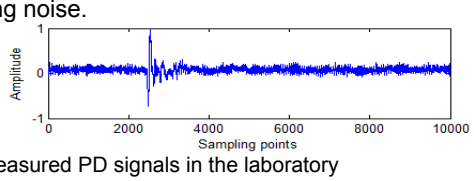


Fig. 7 Measured PD signals in the laboratory

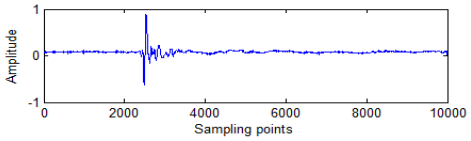


(a) Results of morphological–complex wavelet denoising

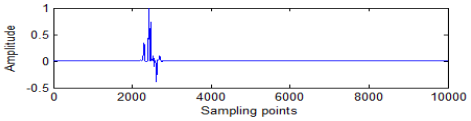


(b) Results of complex wavelet denoising

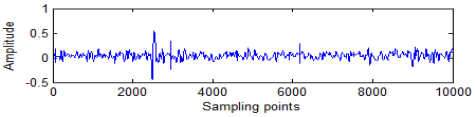


(c) Results of wavelet denoising

Fig. 8 Measured PD signals after denoising

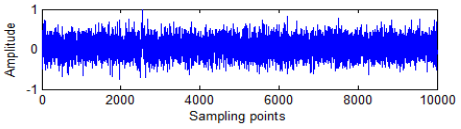


Fig. 9 Measured PD signals in the laboratory

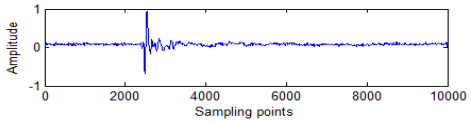


(a) Results of morphological filter–complex wavelet denoising

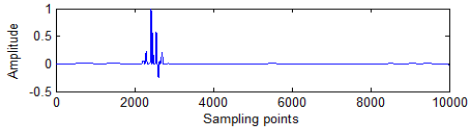


(b) Results of complex wavelet denoising

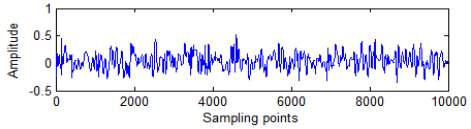


(c) Results of wavelet denoising

Fig. 10 Measured PD signals after denoising

*(B). Denoising Results of the Measured Signal in the Field*

To investigate the rejection capability of the morphological filter–complex wavelet method, denoising analysis was conducted on the PD signals obtained from a switchgear operated in the field.

The measured PD signal, mixed with noise, is shown in Fig. 11. The denoised PD signal is shown in Fig. 12, which shows that the sensitivity of the denoising result in Fig. 12(a) is high and desirable. The denoising results shown in Fig. 12(b) indicates that the loss of signal energy is large and also displays serious signal distortion. The denoising results shown in Fig. 12(c) cannot distinguish the weak PD signal.

From Eq. (16), the noise suppression ratio ( $\rho_{NRR}$ ) of the morphological filter–complex wavelet, which is 105.37 dB, can be obtained. The $\rho_{NRR}$ of the complex wavelet denoising is 74.26 dB, and the $\rho_{NRR}$ of the wavelet denoising is 50.68 dB. Therefore, using the morphological filters–complex wavelet is effective in suppressing periodic narrowband interference and white noise in the PD signal.

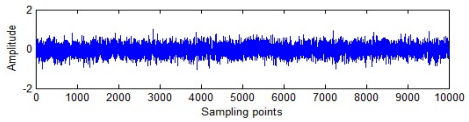


Fig. 11 Measured PD signals under field interference

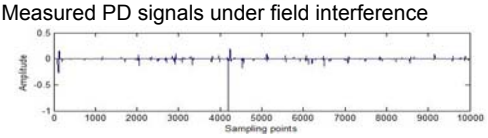


(a) Results of the morphological–complex wavelet denoising

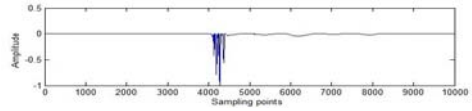


(b) Results of the complex wavelet denoising

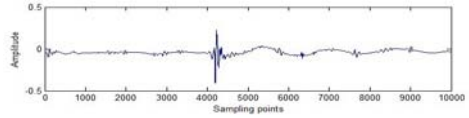


(c) Results of the wavelet denoising

Fig. 12 Measured PD signals after denoising

## Conclusion

(1) This paper has presented a denoising strategy of the interference signal from PD based on mathematical morphology and complex wavelet transform. The morphological filter, which has a flat structural element, and the complex wavelet transform are used in this method to remove the noisy signal in PD to obtain finally the real PD signal.

(2) The denoising results of the measured and the simulated PD signals indicate that the inhibiting ability of this method for periodic narrowband and white noise interferences is better than the wavelet-denoised and the complex wavelet-denoised signals, and the energy loss is smaller, favorable to the restoration of real PD signals.

## REFERENCES

[1] Tang, J.; Sun, C.X.; et al. Application of Wavelet Packet Transform to the Suppression of White-noise and Periodic Narrowband Interference in Partial Discharge Signals. High Voltage Engineering, 2002,28(12):8-10

[2] Wang, X.X.; Sun, S.X.; Ma, D.G. Suppression of periodic pulse interference in on-line PD monitoring systems. Transformer，2002，39(S1)：36-38

[3] Tang, J.; Gao, L.; Xie, Y.B.; et al. Suppressing PD's Periodicity Narrow Band Noise in the PD Measurement by Using Complex Wavelet Packet Transform. High Voltage Engineering, 2008,34(11):2355-2361

[4] Xu, S.Z.; Zhu, Z.S.; Qin, S.L.; et al. Suppression of the periodic pulse shaped interference for on-line PD monitoring. High Voltage Engineering，2001，27(1):32-34

[5] Liu, Y.P.; Lv, F.C.; Li, C.R.; et al. Study of the Mathematical Morphological Filter in Suppressing Periodic Narrow Bandwidth Noise of PD. Proceeding of the CSEE, 2004,24（3）：169-173

[6] Chen, P.; Li, Q.M.; Design and analysis of mathematical morphology-based digital filters. Proceedings of the CSEE，2005，25(11)：60-65

[7] Bi, W.M.; Tang, J.; Yao, C.G.; et al. Simulation and experiment study on wavelet packet decomposition based on entropy threshold for DSI rejection of PD. Proceedings of the CSEE, 2003, 23(5):128-131

[8] Cheng, W.L.; Guo, Y.X.; Wang, J.; et al. Application of Fast Fourier Transform and Generalized Morphological Filter in Suppression of Narrow-Band Interference in Partial Discharge Signal. Power System Technology, 2008,32(10):94-97

[9] Li, T.Y.; Yang, M.; Zhou, X.C.; et al. Method of Partial Discharge Signal Analysis Based on Wavelet Transform and Mathematical Morphology. Power System Technology, 2007,31(6):56-60

[10] Cui, Y. The method of mathematical morphology and applications. Beijing: Science Press,2000

[11] Yin, W.Q.; Liu, Q.J. Mathematical Morphology Review and Its Application in Power System.Relay,2007,35( 19) : 76-83

[12] Chen, X.X. Complex compactly supported orthonormal wavelets and their applications in power system. Proceeding of the CSEE, 2000, 20(7): 83-88

[13] Tang, J.; Xie, Y.B.; Zhu, W.; et al. Suppression of narrowband interference with EWC threshold method for complex wavelet transform. Automation of Electric Power Systems, 2005, 29(7): 43-47

[14] Tang, J.; Peng, L.; Xie, Y.B. An Algorithm of Complex Multilevel Threshold for Reducing White-noise .Proceedings of the CSEE, 2007, 27(21): 25-30

[15] Zhou, X.; Zhou, C.; Kemp I J. An improved methodology for application of wavelet transform to partial discharge measurement denoising. IEEE Transactions on Dielectric and Electrical Insulation, 2005, 12(3): 586-594

[16] Werle P, Akbari A, Borsi H, et al. Enhanced online PD evaluation on power transformers using wavelet techniques and frequency rejection filter for noise suppression[C] //Conference Record of the the 2002 IEEE International Symposium on Electrical Insulation. Boston, MA, USA: IEEE, 2002: 195-198

[17] Tang, J.; Gao, L.; Peng, L.; et al. Study on new evaluation parameters for denoising performance of non-stationary oscillating partial discharge signals. High Voltage Engineering, 2007, 33(12): 66-70